Topography, melting, and viscosity near the core-mantle boundary

Marco Via
November 14, 2008
Advisor: Saswata Hier- Majumder
GEOL 394

Abstract:

Melting and viscosity near the core-mantle boundary are very important parameters that make possible the existence of a topography at the ultralow velocity zone (ULVZ) near the core-mantle boundary(CMB). Consequently, the topography forms permanent mantle plumes that rise to the top of the upper mantle. This paper tests the hypothesis " *The extent of melting in the Ultra Low Velocity Zone near the CMB is less than the rheologically critical melt fraction (RCMF)"*.

The ULVZ is an area of interest for mantle flow convection and it is studied using different approaches, such as numerical experiments and laboratory scaled models. Different studies indicate that a dense layer with low viscosity is likely to display local topographic bumps at the base of mantle plumes **[1, 2] .** Based on these results, we treat the ULVZ as a thin, dense, low viscosity layer between the lower mantle and the liquid outer core. In our gravity current model, the flux of the surrounding lower mantle lifts up the denser, self gravitating layer, thus creating the local bumps in the ULVZ topography. Using the gravity current model, we establish a scaling relationship between the local topographic bumps and the viscosity of the ULVZ. We compare the calculated topography from seismic observations recorded at the Warramanga Array near Australia **[3, 4]** and use the combined dataset to estimate the ULVZ viscosity.

In recent years seismic observations from earthquake events show reductions of S and P waves of 30% and 10% respectively near the ULVZ **[2-5],** indicating possible partial melting in the ULVZ. In addition, these observations also display the existence of ULVZ pockets with an approximate 10% increase in density with an average thickness of 10 km **[2,6-10].** Researches done on melt fraction suggested that the ULVZ contains partial melt although the extent of melting varies widely from 5% to 30% melt fraction **[2, 5, 7].** Laboratory experiments indicate that the viscosity of a partially molten aggregate is substantially reduced if the aggregate contains a melt fraction higher than the rheologically critical melt fraction (RCMF), typically 25%-30% for mantle rocks. We estimated the effective ULVZ viscosity for 30% melt fraction using Einstein-Roscoe equation **[11].** The ULVZ viscosity from the gravity current model was compared with the viscosity predicted by the Einstein-Roscoe equation. The comparison indicates that the viscosity of the ULVZ is lower than the lower mantle viscosity but much higher than the viscosity of the melt therefore the melt fraction must be above the RCMF. Supporting the hypothesis of this project even though it needs future analysis and also more parameters need to be analyzed as variables in the equations used for this paper.

Introduction:

For science in general and geology in particular it is important to understand the thermal evolution of the Earth. The existence of a layer atop the liquid outer core and the lower mantle is a subject of recent research. Seismic data analysis have shown the presence of discontinuities between the upper and lower mantle regions around 660 km deep, and the D" layer about 250 km above the CMB layer **[12]**.

The D" layer has a heterogeneity which is observed as a discontinuity in the seismic reflection of S and P waves with reduced velocities. The uncertainty on rheological composition, temperature changes, pressure changes, melt fraction composition, and

other components make this layer an interesting topic to study and research. Studies have shown that the D" layer could be composed of a thermochmical layer, and a denser-low viscosity layer known as the ultralow velocity zone **[13, 14, 15]**. Also it is known through seismic observation that in the ULVZ P-waves and S-waves velocities are reduced by 10% and 30% respectively. Furthermore perovskite Pv, was thought to be possibly the most abundant phase in the upper and lower mantle regions inside the earth, during this decade laboratory experiments using better technology have created perovskite's polymorph called postperovskite at temperatures of about 2500 K and pressures higher than 120 Gpa **[16, 17].** The existence of this new phase can explain seismic discontinuity, S-wave anisotropy, and anti correlation between the anomalies in S-waves and bulk-sound velocities in the D" layer **[16-23]**. However these phases are not stratified as depth increases towards the CMB layer, because of changes in temperatures in different regions around the planet due to oceanic slab subduction. This assumption implies that lenses of post-perovskite could exist in the D" layer **[6]**.
Seismic observations indicate that the ULVZ has a topography ranging from 5-40 km **[3, 4]**, **[10],[18],** a ratio of 3:1 velocity reduction between P and S waves , and 10% increase in density **[3-5], [10, 18]**
These new findings confirm the complexity of D" but they also have giving us the necessary tools to understand how this region works and helps to the thermal evolution of the planet.

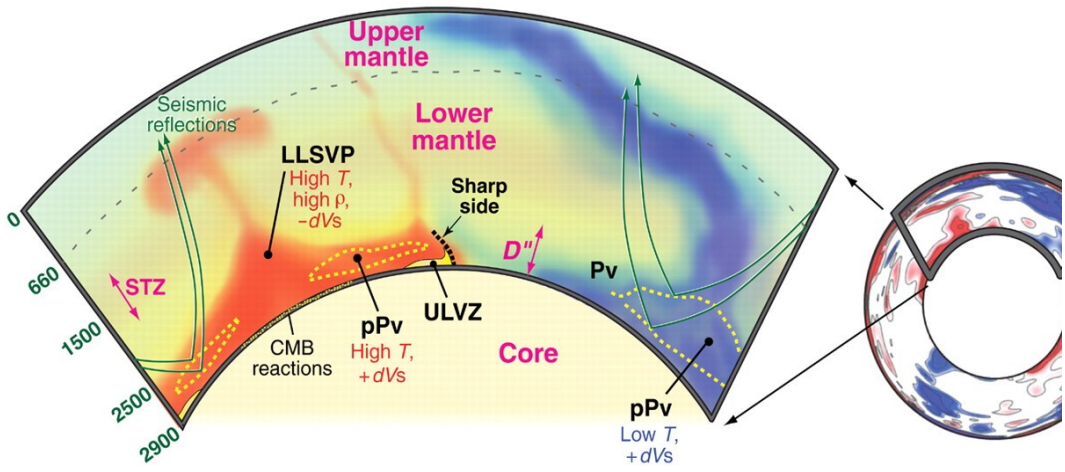

Illustration 1: Cross section of the planet. Showing the possible rheological composition of the lower mantle, and variations of temperatures near the CMB (Garnero, McNamara 2008)

Objectives of Research:

The data of topography, and viscosity values obtained from the numerical code were used to be compared with an average of real topographic seismic data found in the Warramanga Array near Australia **[3, 4].** In order to find a realistic viscosity value based on this topography. The viscosity value for an average thickness of the ULVZ was used

to find a melt fraction using Einstein-Roscoe equation **[11].** By analyzing these results indicate that the topography of the ULVZ has a low viscosity value compared to the lower mantle as well as an increase of density of this layer, confirming other experiments. This in turn implies that the melt fraction value is above the rheologically critical melt fraction. We used studies of melt fraction of peridotites and by including values found in this paper and knowing that when crystals are still in contact in the molten phase the melt fraction value ϕ is greater than the RCFM > 0.35, this molten phase experiences a drastic drop in viscosity, therefore making the ULVZ incapable of developing a thickness above the CMB. The numerical results also show that the flux mass above the ULVZ could not exist if there is no topography implying that mantle plumes will not develop at the base of the lower mantle as shown in other mathematical experiments as well as laboratory experiments **[1, 2][18][24, 25].**

Research Data:

The map below shows the Warramanga Array area in Australia. This work provided the data that we used to compare topography of the ULVZ **[3]**.

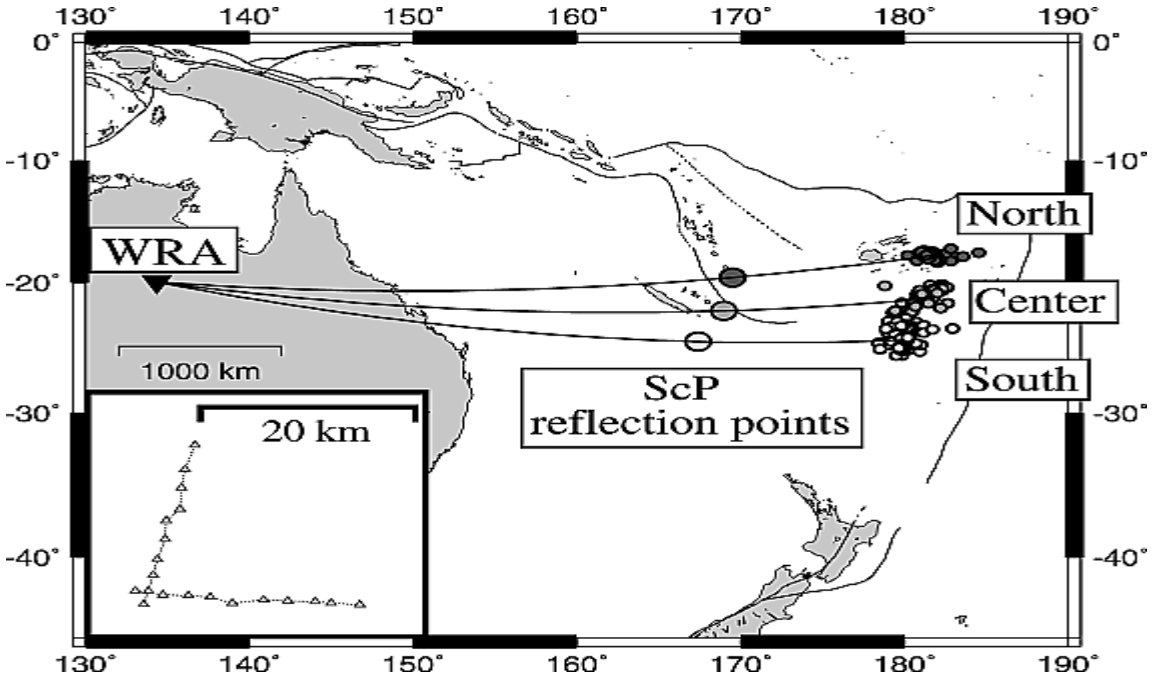

Illustration 2: Tonga-Fiji region, showing earthquakes (small circles), and WRA

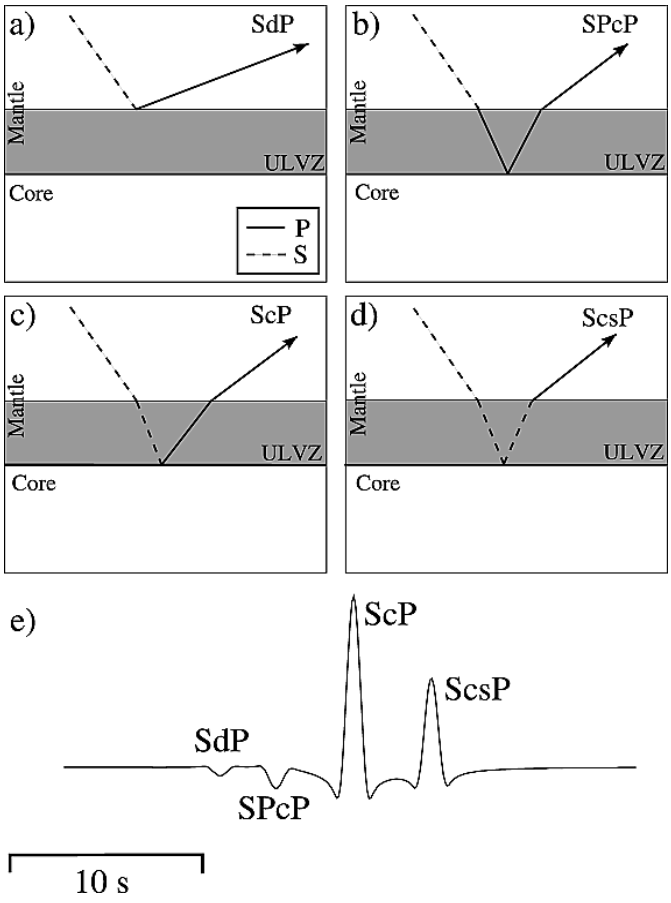

Illustration 3: Shows additional seismic phases. (Rost, and Revenaugh 2004)

Analysis and filtering of seismic data collected at the Tonga-Fiji region was based on the deflection of ScP waves (8),(9). Illustration 5 shows how ScP waves are refracted at the ULVZ, and why these shear wave velocities are useful to map this region at the core-mantle boundary layer and see these additional phases generated by ULVZ layer at the CMB. (a) SdP is the reflection at the top of the ULVZ. (b) SPcP is the conversion of the incident S wave to a P wave at the top of the ULVZ. (c) The main phase ScP is converted off the CMB as a S wave and is converted from S wave to a P wave at the CMB. (d) ScsP is reflected off the CMB as a S wave and is converted to a P wave at the top of the ULVZ on the way up. (e) shows a synthetic sismogram of these additional phases. The modeled ULVZ is 15 km thick with 10% and 30% P wave and S wave velocity reductions, respectively, and a 10% density increase. This synthetic seismogram was obtained by using Gaussian beam tracing **[3].**

The results found above were used to match real seismic data of the ULVZ in the Tonga-Fiji region shown in the chart below.

Table 1. Thickness of ULVZ in the Tonga- Fiji region (7),(8)

Event	Origin Date	Depth (km)	Thickness h (km)
1	29 January 1979	506	8
2	3 July 1979	466	5
3	12 November 1979	573	10
4	9 December 1979	530	20
5	9 February 1980	543	5
6	15 April 1980	449	9
7	15 September 1980	499	8
8	1 January 1981	514	11
9	8 February 1981	538	9
10	3 May 1981	457	10
11	17 August 1981	387	17
12	18 October 1981	509	9
13	9 February 1982	505	8
14	21 February 1982	510	12
15	6 September 1984	540	11
16	20 September 1984	503	9
17	14 March 1985	520	5
18	13 October 1985	501	7.5
19	24 July 1986	549	7
20	10 September 1979	482.5	4
21	20 November 1979	530.3	7
22	24 November 1979	583.3	19
23	6 January 1980	504.9	16
24	20 May 1980	531.8	33
25	11 September 1980	507.8	6
26	18 July 1984	575	4
27	21 February 1985	530.6	8
	Average thickness==>		10.28

The average value found for the thickness of the ULVZ from this paper fits between the predictions of many other researches and numerical experiments which give the ULVZ a thickness of 5 to 40 km. The 10.3 km value was used to match the topography values from the numerical experiments run in scilab.

In the final step of this project data from the following graph was used in order to find a realistic viscosity for the melt.

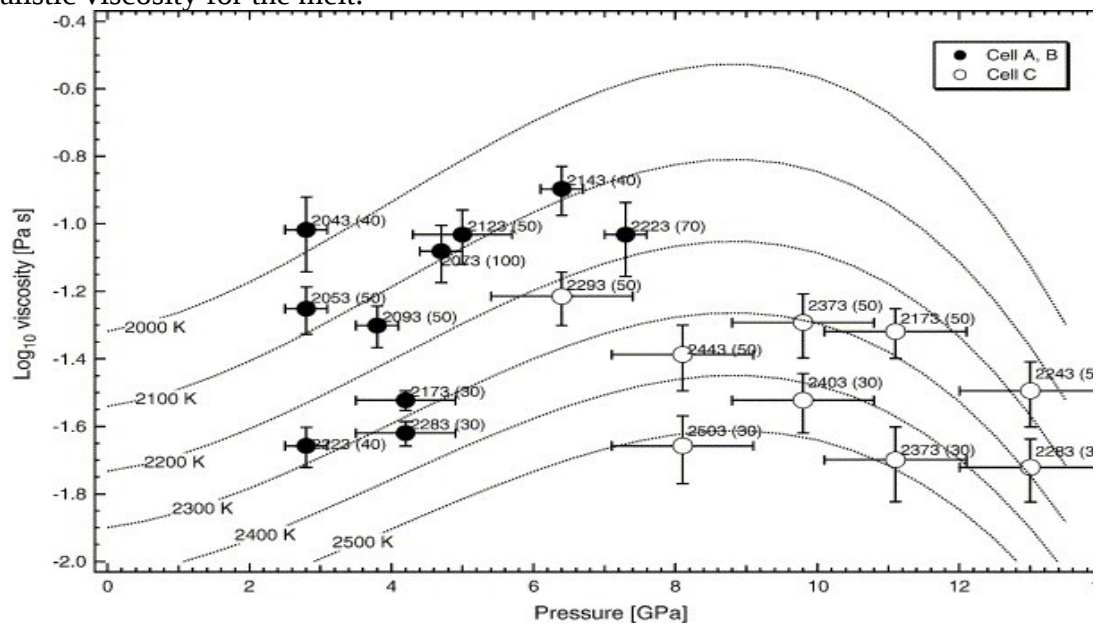

Illustration 4:

Text 1: Experimentally determined viscosities as a function of pressure (Liebske, et al 2005)

Experiment Design:

The first assumption taken in order to write a feasible numerical code was to treat the ULVZ as a thin, dense gravity current, spreading under its own weight. Because of the thickness of the layer is much lower compared its lateral extent, the lubrication theory provides an appropriate model for this layer. We assumed also that the velocity within the layer is mostly in the x-y axis and only varies across the layer. The following governing equation represents the flow within the dense, thin, low viscous layer at the base of a plume.

$\mu \frac{d^2u}{dz^2} = and\ \rho g \nabla_H h$ [Eq. 1] Where; μ *is viscosity of the ULVZ*, ∇_H *is the horizontal gradient operator, defined parallel to the walls of the narrow TBL*, *z is the datum elevation at the CMB*, $\Delta\rho$ *is the viscosity of the ULVZ*, *g is the gravity constant*, and *h is the maximum topography of the ULVZ*

Illustration 5, a simple model of the ULVZ between the lower mantle and the outer core.

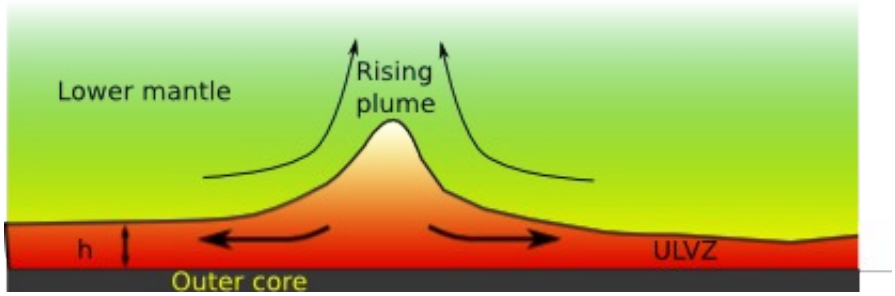

Integrating using the boundary conditions of zero velocity and zero shear stress above the ULVZ we have:

$\frac{\partial \mu}{\partial z}=0$ and $\mu=0$ at $z=0$ The solution is, $\mu=\frac{\Delta \rho g}{2\mu}\nabla_H h z^2$ [Eq. 2]

==> $\frac{\partial h}{\partial t}+\nabla_H * q=\varphi\,\delta(x-x_0)$ [Eq.3] Where q is the volume flux per unit channel area,

defined as, $q=\partial_0^h \mu\, dz$ [Eq.4] , δ is a sink term indicating suction of material into the

plume conduit, and φ is the mass flux into the plume conduit.

Which becomes, $q=\frac{\Delta \rho g h^3}{6\mu}\nabla_H h=\frac{\Delta \rho g}{24\mu}\nabla_H h^4$ [Eq. 5]
combining equations 3 and 5 we obtain,

$\frac{\partial h}{\partial t}+\frac{\Delta \rho g}{24\mu}\nabla_H^2 h^4=\varphi\,\delta(x-x_0)$ [Eq. 6]
In the steady state, $\nabla_H h^4=\frac{24\mu}{\Delta \rho g}\varphi\,\delta(x-x_0)$ [Eq. 7]
Non dimensionilizing the terms,

$h=L\,h*.$, $\nabla=\frac{1}{L}\nabla *.$, $\delta=\frac{\delta *.}{L^2}$ then equation 7 becomes,

$\nabla^2 h^4=\frac{24\mu}{\Delta \rho g}\frac{\varphi}{L^4}\delta$ [Eq. 8] then the intrusion number is defined as

$I=\frac{24\mu}{\Delta \rho g}\frac{\varphi}{L^4}\delta$ [Eq. 9]
finally equation 8 becomes, $\nabla^2 h^4=I\,\delta$ [Eq. 10]

Equation 10 was used to write the scilab numerical code which enable us to find a maximum topography (h) for the ULVZ.

The results of elevation and viscosity values from the numerical experiments are shown in the chart below, after variables were redimensionalized

Table 2: Scilab code values.

Elevation (km)	Intrusion number	Viscosity $1.0\,E^{(+19)}$ (Pa s)
0.26	4.50	0.0000269
1.50	5.83	0.0311929
10.73	7.17	82.285893
91.23	8.50	429536.46

The results are shown below as topographic mounds for different intrusion numbers showing the maximum topography of the ULVZ layer.

Illustration 6: 3-D figures generated by scilab.

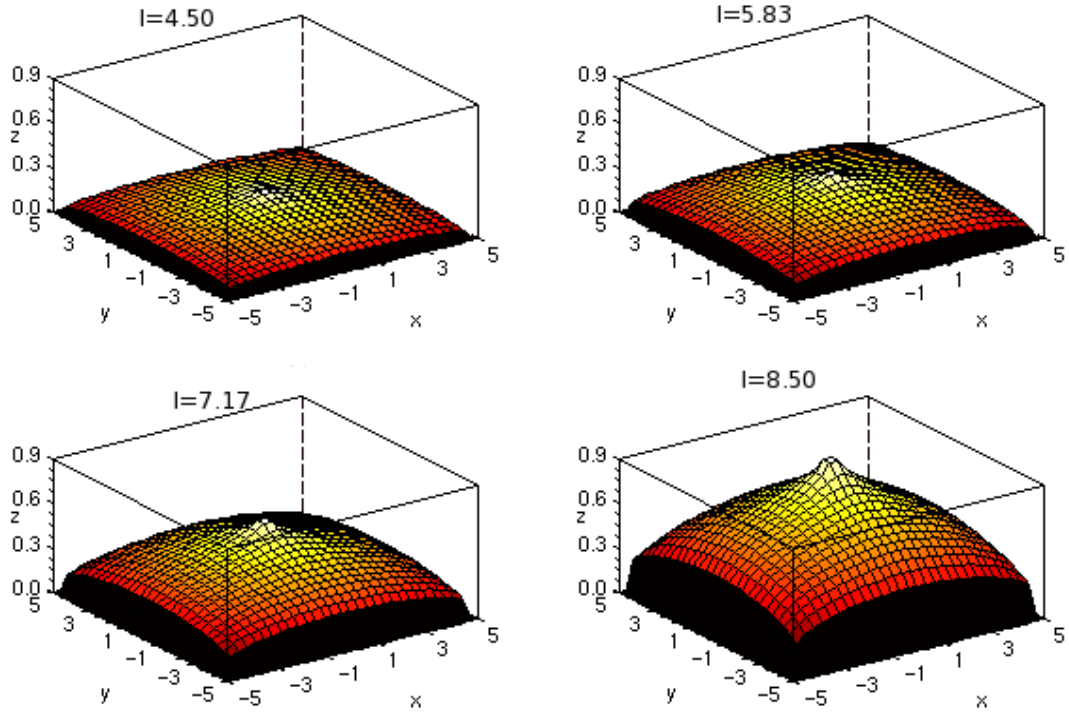

The buoyancy flux is defined as $B=Q_p(\rho_m-\rho_p)$ where Q_p is the volume flux of plume, ρ_m is the density of the mantle, and ρ_p is the density of the plume. We are using the letter Q in order to maintain the terminology about flux. The units for buoyancy flux are $(kg\,s^{-1})$. In order to obtain Q_p I used the following formula: $Q_p=\frac{-B}{\rho_m \alpha_v (T_p-T_1)}$ where $\rho_m=3300(kg/m^3)$ $T_p-T_1=200(K)$

From this analysis of buoyancy flux it was obtained a realistic mass flux value, the buoyancy flux values are obtained based on surface change due to pressure in regions

where we have crust deformation. Based on the initial conditions for the derivation of the equations it was assumed that mass flux is the same at the bottom of the plume or at the dome near the crust surface. The value used for this paper will be worked based on the following data **[26].**

Table 3:

Hotspot Locations	**B (Buoyancy flux) [** $10^3 kg\,s^{-1}$ **]**
Afar, Ethiopia	1.2
Easter Island	3.3
Hawaii	7.4
Marquesas Islands	4.0
Tahiti	4.6
Yellowstone	1.5

Shown below is a graph of data points found in the numerical code. These points generated a maximum topography for viscosity values.

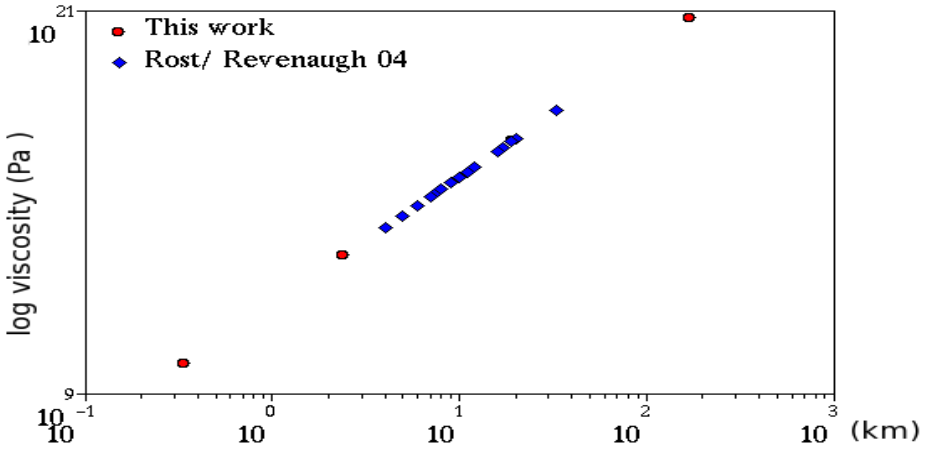

Illustration 7: Viscosity vs Topography from numerical results from this study and seismic observations.

This thickness value was matched to the results found from the numerical experiments in order to find a viscosity value to be used in the next step.

Using the following Einstein-Roscoe equation $\mu_{rock} = \mu_{liq}(1.35\phi - 0.35)^{(-2.5)}$ where, $\mu_{rock}, and\ \mu_{liq}$ are the viscosities of rock (ULVZ) found from numerical code, and liquid (melt) obtained from **[27]**, we found ϕ as the melt fraction in the ULVZ.

Table 4. Melt fraction value.

$\mu(ULVZ)[Pa\,s]$	$\mu(melt)[Pa\,s]$	ϕ
14.1	0.01	0.3

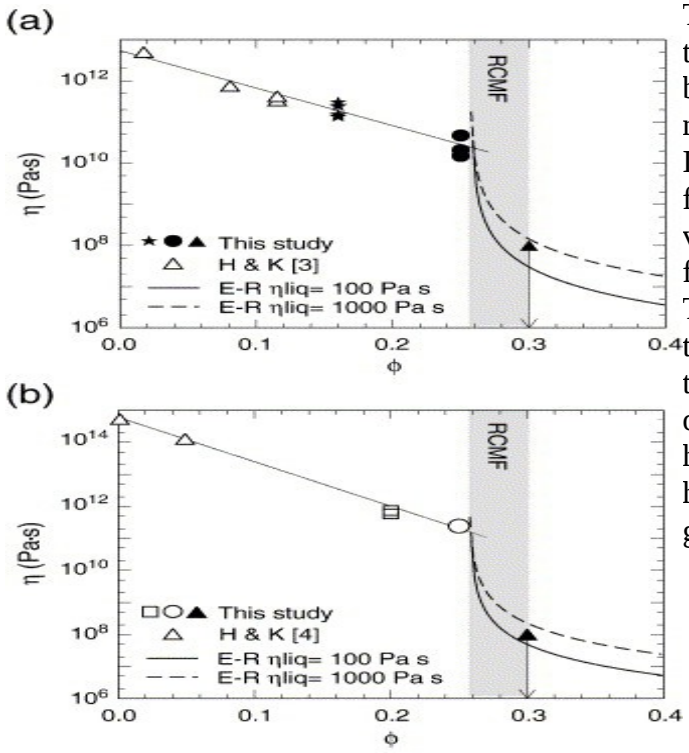

Illustration 8: Viscosity vs. melt fraction for a) 10um, and b) 50um grains

This value is used to be compared in the graph were RCMF is the boundary between a partially molten rock and a molten rock.
In this next step the analysis of melt fraction values obtained from viscosity values are plotted in the flow law graph.
The melt fraction value obtained in this paper will have to be plotted to the left of the RCMF vertical line in order to demonstrate that the hypothesis presented is possible. At higher values of Φ the ULVZ will get depleted.

Demonstrate feasibility:

Comparing and matching numerical experimental results with real seismic data, laboratory experiments, and graphs enable us to find a suitable melting fraction value to test the hypothesis stated above.

Budget:

Computer laboratory in the CSS building on Maryland University campus were used in this project, the use of scilab software and printing costs were paid by the geology department.

Conclusions:

This project was made as an attempt to understand how the ULVZ affects the thermal evolution of our planet. The topography of the ULVZ found through numerical experiments were compared to real seismic observations, this results gave us the opportunity to find viscosity values that might exist in this region. Using a relationship of viscosity and melt fraction between the mantle and the ULVZ we came to a conclusion that a partially molten ULVZ layer is capable of becoming stable enough to resist the flux of the thermochemical layer flowing above the ULVZ, giving the possibility of formation of stable plumes rising to the top of the upper mantle region. Future studies will need to be performed to either confirm or change direction of this topic. The existence of plumes rising from the ULVZ to the upper mantle is still not understood in full but attempts through computer modeling research and laboratory experiments are giving scientists new insight of how this region works and its undeniable influence with the thermal evolution of our planet.

Appendix:

The scilab numerical code written for this project is shown below in order to offer a better understanding to the reader.

Title: scilab_fall_08 CSS Bldg. University of Maryland, College Park

```
clear;
xbasc()
stacksize(100000000);
ngrid=30;
nparam=4;
f=zeros(ngrid,ngrid);
f1=f;
A=zeros(ngrid*ngrid,ngrid*ngrid);
gridx=f;
gridy=f;
delta=f;
rhs=zeros(1,ngrid*ngrid);
xmax=5;
x=linspace(-xmax,xmax,ngrid);
y=linspace(-xmax,xmax,ngrid);
h=(max(x)-min(x))/ngrid;
topo=ones(1,nparam);
intrusion=linspace(6,9,nparam);
//Set up the grid
for ii=1:ngrid;
      gridx(ii,1:ngrid)=x(1:ngrid);
      gridy(:,ii)=y';
end
//Prescribe delta
for ii=1:ngrid;
      for jj=1:ngrid;
      delta(ii,jj)=-h.^2.*exp(-(gridx(ii,jj).^2+gridy(ii,jj).^2)/0.01);
      end
end

for kk=1:nparam //loop through different intrusion number
  delta=intrusion(kk).*delta;
  delta(1,:)=0.0; //boundary condition for the top boundary
  delta(ngrid,:)=0.0;//bottom
  delta(:,1)=0.0;//left boundary
  delta(:,ngrid)=0.0;//right boundary
  //fill up the rhs vector
  for ii=1:ngrid
    rhs((ii-1)*ngrid+1:ii*ngrid)=delta(ii,1:ngrid);
  end


    //Fill up the matrix A
    for ii=1:ngrid*ngrid,
        //The Laplacian operator
        A(ii,ii)=-4.0;
        if(ii<ngrid*ngrid) then
        A(ii,ii+1)=1.0;
        end
        if (ii>1)  then
```

```
        A(ii,ii-1)=1.0;
        end
        if(ii<ngrid*(ngrid-1)) then
        A(ii,ii+ngrid)=1.0;
        end
        if(ii>ngrid) then
        A(ii,ii-ngrid)=1.0;
        end
    end
    //Now the boundary conditions
  A(1:ngrid,:)=0.0;
//    //Top
    A(ngrid*(ngrid-1)+1:ngrid*ngrid,:)=0.0;
      for ii=1:ngrid
        for jj=1:ngrid
          if(ii==jj) then
          A(ii,jj)=1;
          end
        end
      end
      //Bottom
      for ii=ngrid*(ngrid-1):ngrid*ngrid
        for jj=ngrid*(ngrid-1):ngrid*ngrid
          if(ii==jj) then
          A(ii,jj)=1.0;
          end
        end
      end
  for ii=2:ngrid-1
      A((ii-1)*ngrid+1,:)=0.0;
      A((ii-1)*ngrid+1,(ii-1)*ngrid+1)=1.0; //left
      A(ii*ngrid,:)=0.0;
      A(ii*ngrid,ii*ngrid)=1.0; //right
      end
    //Solve for u
  B=inv(A);
    u=B*rhs'; //the ' changes a row vector to a column vector
    //[u,B]=linsolve(A,-rhs');
    //fill up the solution vector into the matrix
    f=zeros(ngrid,ngrid);
    for ii=1:ngrid
    f(ii,1:ngrid)=u((ii-1)*ngrid+1:ii*ngrid)';
    end
    xset("window",0)
    f1=f;
    f=sqrt(sqrt(f));
    topo(1,kk)=max(f1);
    xset('colormap',hotcolormap(128))
    subplot(sqrt(nparam),sqrt(nparam),kk)
    surf(gridx,gridy,f)
    a=gca("current_axes");
    a.data_bounds=[-xmax,-xmax,0;xmax,xmax,0.8];
    xtitle(string(intrusion(kk)),'x','y','z')
  end
  delT=200; //K
  rhom=3300; //kg/m^3
  B=7.4e3;//kg/s
```

```
  alpha=3e-5;// 1/K
  Qp=B/rhom/alpha/delT; //m^3/s
  drho=O.1*556O;//kg/m^3
  L=1e5;//m
  g=1O;//m/s^2
  mu=drho.*g.*(topo.*L).^4./24./Qp; //pas
  topo=topo.*L; //km
  xset("window",1)

  plot2d(topo./1e3,mu,-9,logflag="ll")
  xset("font",2,4)
  b=gca();
  b.children.children(1).mark_background=5;
  //Qp=373.73 //m^3/s
  rost=
[8,5,1O,2O,5,9,8,11,9,1O,17,9,8,12,11,9,5,7.5,7,4,7,19,16,33,6,4,8].*1e
3;
    murost=rost.^4*drho.*g/24./Qp;
  //xset("window",1)
  plot2d(rost./1e3,murost,-5,logflag="ll")
  b=gca();
  b.children.children(1).mark_background=2;
  legend(['This work' 'Rost/ Revenaugh O4'],2,boxed=%f)
  xtitle('','h(km)','log(viscosity) (Pas)')
  a=get("current_axes");
  a.x_label.font_size=4;
  a.x_label.font_style=2;
  a.y_label.font_size=4;
  a.y_label.font_style=2;
```

Bibliography

[1]Jellinek, M. A., and Manga, M. (2004) Links between long-lived hot spots, mantle plumes, D", and plate tectonics. *American Geophysical Union.* v. 42, 1-35.

[2]Garnero, E. J. (2000) Heterogeneity of the Lowermost Mantle. *Earth.Planet.Science.* v. 28, 509-537.

[3]Rost, S., and Revenaugh, J. (2003) Small-scale ultralow- velocity zone structure imaged by Sc P. *Journal of Geophysical Research*. v. 108, 1-10.

[4]Rost, S., and Revenaugh, J. (2001). Seismic Detection of Rigid Zones at the Top of the Core. *Science*. v. 294, 1-8.

[5]Rost, S., Garnero, E. J., Williams, Q. and Manga, M. (2005) Seismological constraints on a possible plume root at the core-mantle boundary. *Nature Publishing Group*. v. 435, 666-669.

[6]Garnero, E., and McNamara, A. (2008) Structure and Dynamics of Earth's Lower Mantle. *Science.* v. 320, 626-628.

[7]Lay, T., Garnero, E. J., and Williams, Q. (2004) Partial melting in a thermo-chemical boundary layer at the base of the mantle. *Physics of the Earth and Planetary Interiors.* v. 146, 441-467.

[8]Thorne, M. S., and Garnero, E. J. (2004) Inferences on ultralow-velocity zone structure from a global analysis of *SPdKS* waves. *Journal of Geophysical Research*. v. 109, 1-22.

[9]Ross, A. R., and Thybo, H. (2004) Reflection seismic profiles of the core-mantle boundary. *Journal of Geophysical Research*. v. 109, 1-19.

[10]Wen, L., and Helmberger, D. V. (1998) Ultra-Low Velocity Zones Near the Core-Mantle Boundary from Broadband PKP Precursors. *Science Magazine.* v. 279, 1701-1703.

[11]Scott, T., and Kohlstedt, D. L. (2006) The effect of large melt fraction on the deformation behavior of peridotite. *Earth and Planetary Science Letters*. v. 246, 177-187.

[12]Wysession, M. E., Lay, T., Revenaugh, J., Williams, Q., Garnero, E. J., Jeanloz, R., and Kellogg, L. H. (1998) The D" Discontinuity and its implications. *American Geophysical Union.* v. 28, 273-297.

[13]Anderson, D. L. (1998) The EDGES of the Mantle. *Geodynamics.* v. 28, 255-271.

[14]Namiki, A. (2003) Can the mantle entrain D"?. *Journal of Geophysical Research.* v. 108, 1-11.

[15]Leng, W., and Zhong, S. (2008) Controls on plume flux and plume excess temperature.. *Journal of Geophysical Research*. v. 113, 1-15.

[16]Hirose, K. (2007) Discovery of Post-Perovskite Phase Transition and the Nature of D" Layer. *Geophysical Monograph Series.* v. 174, 19-32.

[17]Yagi, T. (2007) Review of experimental studies on mantle phase transitions. *American Geophysical Union*. v. 174, 9-18.

[18]Kellogg, L. H., and King, S. D. (1997) The effect of temperature dependent viscosity on the structure of new plumes in the mantle: Results of a finite element model in a spherical, axisymmetric shell. *Earth and Planetary Science Letters.* v. 148, 13-26.

[19]Buffet, B. A., Garnero, E. J., and Jeanloz, R. (2000). Sediments at the Top of Earth's Core. *Science.* v. 290, 1338-1342.

[20]Hutko, A. R., Lay, T., Revenaugh, J., and Garnero, E. J. (2008) Anticorrelated Seismic Velocity Anomalies from Post-Perovskite in the Lowermost Mantle. *Science.* v. 320, 1070-1074.

[21]Labrosse, S. Hernlund, J. W., and Coltice, N. (2007) A crystallizing dense magma ocean at the base of the Earth's mantle. *Nature Publishing Group.* V. 450, 866-869.

[22]Yamazaki, D., and Karato, S. (2001) Some mineral physics constraints on the rheology and geothermal structure of Earth's lower mantle. *American Mineralogist.* v. 86, 385-391.

[23]Kellogg, L. H. (1997) Growing the Earth's D" layer: Effect of density variations at the core-mantle boundary. *Geophysical Research Letters.* v. 24, 2749-2752.

[24]Tackley, P. J. (1998) Three- Dimentional Simulations of Mantle Convection with a Thermo-Chemical Basal Boundary Layer: D". *Geodynamics.* v. 28, 231-252.

[25] Olson, P. (____) Hot spots, swells and mantle plumes. *Department of Earth and Planetary Sciences.* v. 3, 33-51.

[26]Turcotte, Donald L., and Schubert Gerald. Geodynamics. Second ed. New York, NY: Cambridge University, 2002. 259-61.

[27]Liebske, C., Schmickler, B., Terasaki, H., Poe, B. T., Suxuki, A., Funakoshi, K., Ando, R., and Rubie, D. C. (2005) Viscosity of peridotite liquid up to 13 Gpa: Implications for magma ocean viscosities. *Earth and Planetary Science Letters.* v. 240, 589-604.